AIMS Mathematics, 11(5): 14457–14473.
DOI: 10.3934/math.2026592
Received: 03 April 2026
Revised: 07 May 2026
Accepted: 12 May 2026
Published: 22 May 2026

http://www.aimspress.com/journal/Math

Research article

Global properties of an HIV model with cytokine enhancement, saturated incidence and distributed delays

Cuifang Lv[1,*], Xiaoyan Chen[2] and Chaoxiong Du[1]

[1] School of Mathematics Science, Changsha Normal University, Changsha 410100, China
[2] School of Mathematics, Changsha University, Changsha 410022, China

* **Correspondence:** Email: lvgod0729@126.com.

Abstract: This paper analyzes the global dynamics of an Human Immunodeficiency Virus (HIV) delay model which incorporates cytokine enhancement and three saturated incidence rates. Based on the distinct thresholds of two reproduction numbers, we establish the existence of both immunity-inactivated and immunity-activated equilibria. Furthermore, the global attractivity of all three equilibria is rigorously established through constructing Lyapunov functionals. Our simulations demonstrate the following: (i) enhanced virus-cell saturation demonstrates a superior efficacy over the saturation effect of inflammatory cytokines in driving systemic parameters toward Acquired Immunodeficiency Syndrome (AIDS) amelioration; (ii) immune saturation can critically impair anti-HIV defense mechanisms; (iii) increasing the virus-cell saturation levels significantly neutralizes the adverse effects of immune saturation on disease progression; and (iv) time delays exhibit therapeutic benefits within an optimal range, with diminishing returns beyond this threshold. These results suggest both saturation parameters and time delays represent potential therapeutic targets for HIV treatment.

Keywords: cytokine enhancement; saturated incidence; distributed delay; stability
Mathematics Subject Classification: 34D20, 34D23, 92B05

1. Introduction

The Human Immunodeficiency Virus (HIV) represents a major global public health challenge by specifically targeting $CD4^+$ T lymphocytes, thus leading to Acquired Immunodeficiency Syndrome (AIDS) and severe impairment of host immune defenses [1, 2]. A critical manifestation of HIV progression is the sustained decline in $CD4^+$ T helper cell populations, which occurs through three principal cell death pathways: apoptosis, necroptosis, and pyroptosis. Notably, pyroptosis, a caspase-1-dependent inflammatory cell death mechanism, is the predominant form of $CD4^+$ T cell death in HIV infections. Doitsh et al. [3] demonstrated that pyroptosis accounts for up to 95% of $CD4^+$ T cell loss,

which is mediated by the cysteine protease caspase-1. This process establishes a pathogenic feedback loop: Inflammatory cytokines such as IL-1β are released by pyroptotic CD4$^+$ T cells, which then draw significant amounts of uninfected CD4$^+$ T cells towards the areas of inflammation. This chemotactic response paradoxically expands the pool of target cells available for HIV infection, thereby amplifying viral spread and accelerating immune system deterioration.

Recent advances have established pyroptosis as a predominant mechanism underlying HIV-induced CD4$^+$ T cell depletion, thus prompting the development of dynamic models that incorporate this cell death pathway [4–6]. Moreover, upon pathogen invasion, the human body mounts an immune response that is primarily divided into two branches: innate immunity and adaptive immunity [7, 8]. Most existing HIV modeling studies focus on adaptive immunity, which is comprised of the Cytotoxic T Lymphocyte (CTL) immune response and the antibody-mediated humoral immune response. References [9, 10] constructed and analyzed HIV dynamics models by incorporating CTL responses, and systematically examined their dynamic behavior. Notably, Zhang et al. [10] demonstrated that the Hopf bifurcation emerges at the immune-activated equilibrium. Furthermore, Chen et al. [11] investigated a cytokine-enhanced viral infection model by incorporating both CTLs and antibody immune responses. To investigate the role of CTL immune responses in HIV infection, and motivated by the fact that distributed delays more accurately capture the biological realism of the infection process, we previously developed a novel dynamical system that incorporated distributed delays in [12], which is presented as follows:

$$\begin{cases} \dot{x}(t) = \lambda - \beta_1 x(t)c(t) - \beta_2 x(t)v(t) - \mu x(t), \\ \dot{y}(t) = \int_0^\infty f_1(\tau)e^{-m_1\tau}[\beta_1 x(t-\tau)c(t-\tau) + \beta_2 x(t-\tau)v(t-\tau)]\mathrm{d}\tau - (\alpha + d)y(t) - py(t)z(t), \\ \dot{c}(t) = \sigma \int_0^\infty f_2(\tau)e^{-m_2\tau}y(t-\tau)\mathrm{d}\tau - qc(t), \\ \dot{v}(t) = k \int_0^\infty f_3(\tau)e^{-m_3\tau}y(t-\tau)\mathrm{d}\tau - \gamma v(t), \\ \dot{z}(t) = \eta y(t)z(t) - bz(t). \end{cases} \tag{1.1}$$

Here, $x(t)$ and $y(t)$ denote the concentrations of uninfected and infected CD4$^+$ T cells at time t, respectively. Moreover, the concentrations of inflammatory cytokines, viruses, and CTLs at time t are denoted by $c(t)$, $v(t)$, and $z(t)$, respectively. λ represents the productivity of uninfected cells, while β_1 and β_2 describe the infection rates of uninfected cells mediated by inflammatory cytokines and free viruses. The death rates of uninfected and infected CD4$^+$ T cells are denoted by μ and d, respectively, whereas q, γ, and b represent the clearance rates of inflammatory cytokines, viral particles, and CTLs. Infected cells undergo additional pyroptosis-induced cell death at a rate of α. Meanwhile, σ, k, and η describe the proliferation rates of inflammatory cytokines, viral replication, and CTLs, respectively. The factor $e^{-m_1\tau}$ quantifies the survival probability of infected cells (via cytokines or viruses) during the intracellular delay τ before productive infection. Meanwhile, $e^{-m_2\tau}$ and $e^{-m_3\tau}$ describe the fractions of cytokines and virions, respectively, that remain active after their production delay τ.

In HIV infection models, the incidence rate function critically determines viral dynamics by quantifying the probability of successful infections per contact between susceptible CD4$^+$ T cells and free virions. The infection rate between viruses and cells is often simplified to a bilinear form, but this assumption is biologically unrealistic [13]. Viral transmission is regulated by multiple factors, including the immune status of the host cells and the characteristics of the infecting virus. To more realistically describe this process, the saturation incidence rate is widely employed as a functional response to model the nonlinear contact between susceptible cells and free virions [14–17]. Notably,

nearly all existing HIV dynamical models that account for pyroptosis adopt the bilinear incidence rate. Furthermore, the time delays involved in HIV progression for most AIDS patients typically exhibit finite distributed features. To systematically compare the respective roles of saturated incidence rates associated with viruses and inflammatory cytokines during infection, this paper employs incidence functions of the same structural form but with distinct parameter values for modeling and dynamical analyses. In addition, to characterize the saturation effect of the immune response, we introduce a saturation term into the immune function. Accordingly, we propose an improved dynamical model that incorporates both saturated incidence rates and finite distributed delays as follows:

$$\begin{cases} \dot{x}(t) = \lambda - \frac{\beta_1 x(t)c(t)}{1+mc(t)} - \frac{\beta_2 x(t)v(t)}{1+nv(t)} - \mu x(t), \\ \dot{y}(t) = \int_0^{T_1} \frac{f_1(\tau_1)e^{-m_1\tau_1}\beta_1 x(t-\tau_1)c(t-\tau_1)}{1+mc(t-\tau_1)}\mathrm{d}\tau_1 + \int_0^{T_1} \frac{f_1(\tau_1)e^{-m_1\tau_1}\beta_2 x(t-\tau_1)v(t-\tau_1)}{1+nv(t-\tau_1)}\mathrm{d}\tau_1 - (\alpha+d)y(t) - py(t)z(t), \\ \dot{c}(t) = \sigma\int_0^{T_2} f_2(\tau_2)e^{-m_2\tau_2}y(t-\tau_2)\mathrm{d}\tau_2 - qc(t), \\ \dot{v}(t) = k\int_0^{T_3} f_3(\tau_3)e^{-m_3\tau_3}y(t-\tau_3)\mathrm{d}\tau_3 - \gamma v(t), \\ \dot{z}(t) = \frac{\eta y(t)z(t)}{1+\xi z(t)} - bz(t), \end{cases} \tag{1.2}$$

where T_1 represents the upper time limit required for uninfected CD4$^+$ T cells to become productively infected following exposure to inflammatory cytokines and free virions. The parameters T_2 and T_3 denote the maximum time delays for the processes which span from the initial activation of infected CD4$^+$ T cells to the subsequent production of mature inflammatory cytokines and viruses, respectively. $\int_0^{T_1} \frac{f_1(\tau_1)e^{-m_1\tau_1}\beta_1 x(t-\tau_1)c(t-\tau_1)}{1+mc(t-\tau_1)}\mathrm{d}\tau_1$ and $\int_0^{T_1} \frac{f_1(\tau_1)e^{-m_1\tau_1}\beta_2 x(t-\tau_1)v(t-\tau_1)}{1+nv(t-\tau_1)}\mathrm{d}\tau_1$ represent the total number of susceptible cells that become infected through either inflammatory cytokine-mediated mechanisms or direct viral infection, respectively, survive, and then convert into infected cells within the time interval $[0, T_1]$. The term $\frac{\eta y(t)z(t)}{1+\xi z(t)}$ is called the saturated CTL response function. m, n, and ξ are nonnegative constants. Similarly to [12], for $i = 1, 2, 3$, let $f_i(\tau_i) : [0, \infty) \to [0, T_i]$ be probability density functions with compact support (i.e., $f_i(\tau_i) \geq 0$ and $\int_0^{T_i} f_i(\tau_i)\mathrm{d}\tau_i = 1$). For notational convenience, we define the following constants throughout this paper: $k_1 = \int_0^{T_1} f_1(\tau)e^{-m_1\tau_1}\mathrm{d}\tau_1, k_2 = \int_0^{T_2} f_2(\tau)e^{-m_2\tau_2}\mathrm{d}\tau_2$, and $k_3 = \int_0^{T_3} f_3(\tau)e^{-m_3\tau_3}\mathrm{d}\tau_3$.

The content of this study is presented in the following structure: Section 2 establishes the boundedness and non-negativity of solutions, and provides existence conditions for the immune-inactivated and immune-activated equilibria; Section 3 rigorously proves the global attractivity of all three equilibria through the construction of appropriate Lyapunov functionals; in Section 4, we not only apply numerical simulations to validate the stability properties of each equilibrium but also systematically examine how variations in saturation constants and time-delay parameters affect the system's dynamic behavior; and finally, a comprehensive discussion of the study's key findings is presented in Section 5.

2. Preliminaries

Denote $T = \max\{T_1, T_2, T_3\}$ and fix $\delta > 0$. The initial condition for Model (1.2) is given by the following:

$$\psi(\theta) = (\psi_1(\theta), \psi_2(\theta), \psi_3(\theta), \psi_4(\theta), \psi_5(\theta)) \in C_+^5 = \{\psi \in C((-T, 0], \mathcal{R}_+^5)\}, \tag{2.1}$$

where $\|\psi\| = \sup_{\theta\leq 0}|\psi(\theta)|e^{\delta\theta} < \infty$, $\mathcal{R}^5_+ = \{(x_1, x_2, x_3, x_4, x_5) : x_i \geq 0, i = 1, 2, 3, 4, 5\}$. Here, we require that $\psi(\theta)e^{\delta\theta}$ is uniformly continuous for $\theta \in (-T, 0]$. Thus, under initial condition (2.1), following the fundamental theory of functional differential equations [18], Model (1.2) admits a unique solution $(x(t), y(t), c(t), v(t), z(t))$ for all $t > 0$.

Theorem 2.1. *(Positivity and boundedness) For Model* (1.2) *with initial condition* (2.1)*, the solution* $(x(t), y(t), c(t), v(t), z(t))$ *remains strictly positive and uniformly ultimately bounded for all* $t > 0$.

Proof.

$$g(t,\psi) = \begin{pmatrix} \lambda - \frac{\beta_1\psi_1(0)\psi_3(0)}{1+m\psi_3(0)} - \frac{\beta_2\psi_1(0)\psi_4(0)}{1+n\psi_4(0)-\mu\psi_1(0)} \\ \int_0^{T_1} f_1(\tau_1)e^{-m_1\tau_1}\left(\frac{\beta_1\psi_1(-\tau_1)\psi_3(-\tau_1)}{1+m\psi_3(-\tau_1)} + \frac{\beta_2\psi_1(-\tau_1)\psi_4(-\tau_1)}{1+n\psi_4(-\tau_1)}\right)\mathrm{d}\tau_1 - (\alpha+d)\psi_2(0) - p\psi_2(0)\psi_5(0) \\ \sigma\int_0^{T_2} f_2(\tau_2)e^{-m_2\tau_2}\psi_2(-\tau_2)\mathrm{d}\tau_2 - q\psi_3(0) \\ k\int_0^{T_3} f_3(\tau_3)e^{-m_3\tau_3}\psi_2(-\tau_3)\mathrm{d}\tau_3 - \gamma\psi_4(0) \\ \frac{\eta\psi_2(0)\psi_5(0)}{1+\xi\psi_5(0)} - b\psi_5(0) \end{pmatrix}.$$

Since $\psi_i(0) \geq 0$ for $i = 1, 2, 3, 4$, we obtain $g(t, \psi) \geq 0$. According to [19], for any $\psi \in C^5_+$, the solutions of Model (1.2) remain nonnegative on their maximal interval of existence. Now, we establish the boundedness property. Focusing on the first equation of Model (1.2) leads to the following:

$$\dot{x}(t) = \lambda - \frac{\beta_1 x(t)c(t)}{1+mc(t)} - \frac{\beta_2 x(t)v(t)}{1+nv(t)} - \mu x(t),$$

which yields the inequality

$$x(t) \leq x(0)e^{-\mu t} + \frac{\lambda}{\mu}(1 - e^{-\mu t}).$$

Since the initial conditions in (2.1) are non-negative, we derive $\limsup_{t\to\infty} x(t) \leq \frac{\lambda}{\mu}$, thereby demonstrating the boundedness of $x(t)$. Define the following:

$$M(t) = \int_0^{T_1} f_1(\tau_1)e^{-m_1\tau_1}x(t-\tau_1)\mathrm{d}\tau_1 + y(t) + \frac{p}{\eta}z(t);$$

then, obtain the following:

$$\dot{M}(t) \leq \lambda k_1 - \tilde{\mu}M(t),$$

where $\tilde{\mu} = \min\{\mu, \alpha + d, b\}$. Consequently, we have the following:

$$M(t) \leq M(0)e^{-\tilde{\mu}t} + \frac{\lambda k_1}{\tilde{\mu}}(1 - e^{-\tilde{\mu}t}).$$

From the non-negativity conditions in (2.1), we conclude that $\limsup_{t\to\infty} M(t) \leq \frac{\lambda k_1}{\tilde{\mu}}$. Furthermore, we obtain $\limsup_{t\to\infty} y(t) \leq \frac{\lambda k_1}{\tilde{\mu}}$, $\limsup_{t\to\infty} z(t) \leq \frac{\eta\lambda k_1}{p\tilde{\mu}}$. Additionally, we obtain $\limsup_{t\to\infty} c(t) \leq \frac{\lambda\sigma k_1 k_2}{\tilde{\mu}q}$ and $\limsup_{t\to\infty} v(t) \leq \frac{\lambda k k_1 k_3}{\tilde{\mu}\gamma}$. Therefore, the system solutions $x(t), y(t), c(t), v(t)$, and $z(t)$ are uniformly ultimately bounded for all $t > 0$. □

Following the methodology described in [10], we calculate the basic reproduction number as

$$R_0 = \frac{\lambda\sigma\beta_1 k_1 k_2}{\mu q(\alpha + d)} + \frac{\lambda k\beta_2 k_1 k_3}{\mu\gamma(\alpha + d)},$$

which denotes the average number of new $CD4^+$ T cell infections that originate from one initially infected cell when CTL responses are absent. Furthermore, the CTL immunity reproduction number is formally defined as

$$R_1 = \frac{\eta y_1}{b},$$

which quantifies the expected number of secondary CTLs produced by one effector CTL throughout its lifespan.

Model (1.2) admits an infection-free equilibrium, which is denoted by $E_0 = (x_0, 0, 0, 0, 0)$ for $x_0 = \lambda/\mu$. When $R_0 > 1$, suppose that there exists an immunity-inactivated equilibrium $E_1 = (x_1, y_1, c_1, v_1, 0)$ in Model (1.2). Solving the equations in (1.2) yields the following:

$$c_1 = \frac{\sigma k_2 y_1}{q}, \quad v_1 = \frac{k k_3 y_1}{\gamma}, \quad x_1 = \frac{(\alpha + d)(q + m\sigma k_2 y_1)(\gamma + nk k_3 y_1)}{\sigma\beta_1 k_1 k_2(\gamma + nk k_3 y_1) + k\beta_2 k_1 k_3(q + m\sigma k_2 y_1)}.$$

Here, y_1 is determined by solving $F(y) = 0$, where

$$\begin{aligned} F(y) \triangleq\ & \sigma k k_2 k_3 M(\mu mn + N)y^2 + [Mk k_3 q(\beta_2 + \mu n) + M\gamma\sigma k_2(\beta_1 + \mu m) - \lambda\sigma k k_1 k_2 k_3 N]y \\ & + M\mu q\gamma - \lambda\sigma\beta_1 k_1 k_2\gamma - \lambda k\beta_2 k_1 k_3 q, \end{aligned}$$

with $M = \alpha + d$, and $N = \beta_1 n + \beta_2 m$. Since $F(+\infty) = +\infty$ and $F(0) = (\alpha + d)\mu q\gamma(1 - R_0) < 0$ (where $R_0 > 1$), $F(y) = 0$ possesses at least one positive root in $(0, +\infty)$. For the case of two distinct real roots $\tilde{y}_1$ and $\tilde{y}_2$, Vieta's formulas give the following:

$$\tilde{y}_1\tilde{y}_2 = \frac{\mu q\gamma(1 - R_0)}{\sigma k k_2 k_3(\mu mn + \beta_1 n + \beta_2 m)} < 0,$$

which guarantees the existence of a unique positive root $y_1 > 0$ that satisfies $F(y_1) = 0$.

Assuming $R_0 > 1$ and $R_1 > 1$, Model (1.2) admits an immunity-activated equilibrium $E^* = (x^*, y^*, c^*, v^*, z^*)$. Solving Model (1.2) yields the following:

$$c^* = \frac{\sigma k_2 y^*}{q}, \quad v^* = \frac{k k_3 y^*}{\gamma}, \quad z^* = \frac{\eta y^* - b}{b\xi}, \quad x^* = \frac{\lambda\Delta_1\Delta_2}{\sigma\beta_1 k_2 y^*\Delta_2 + \beta_2 k k_3 y^*\Delta_1 + \mu\Delta_1\Delta_2},$$

where $\Delta_1 = q + m\sigma k_2 y^*$, and $\Delta_2 = \gamma + nk k_3 y^*$. The value y^* is determined by solving $G(y) = H(y)$, where

$$G(y) = \frac{1}{p}\left[\frac{\lambda k_1(\beta_2 k k_3\Delta_1 + \sigma\beta_1 k_2\Delta_2)}{\sigma\beta_1 k_2 y\Delta_2 + \beta_2 k k_3 y\Delta_1 + \mu\Delta_1\Delta_2} - (\alpha + d)\right], \quad H(y) = \frac{\eta y - b}{b\xi}.$$

Evidently, $G(y)$ is strictly decreasing with respect to y, with $G(y_1) = 0$ and $G(0) = \frac{(\alpha+d)(R_0-1)}{p} > 0$ (since $R_0 > 1$). $H(y)$ is strictly increasing in y, which satisfies $H(0) = -\frac{1}{\eta}$ and $H(\frac{b}{\eta}) = 0$. Under the condition $R_1 > 1$ (which implies $y_1 > \frac{b}{\eta}$), there exists a unique intersection point $y^* \in (\frac{b}{\eta}, y_1)$ between the curves $G(y)$ and $H(y)$. Based on the above analysis, the subsequent theorem can be established.

Theorem 2.2. (*i*) *Model* (1.2) *always has a unique infection-free equilibrium* $E_0 = (x_0, 0, 0, 0, 0)$. (*ii*) *If* $R_0 > 1$, *then Model* (1.2) *only has equilibria* E_0 *and* $E_1 = (x_1, y_1, c_1, v_1, 0)$. (*iii*) *If* $R_0 > 1$ *and* $R_1 > 1$, *then Model* (1.2) *has three equilibria* E_0, E_1, *and* $E^* = (x^*, y^*, c^*, v^*, z^*)$.

3. Global attractivity of equilibria

Due to the coupling of distributed delays, saturated incidence rates, and the high-dimensional nature of the system, the local stability analysis of the equilibria in this model is mathematically challenging. Therefore, we focus on proving the global attractivity of the equilibria by constructing appropriate Lyapunov functionals and applying LaSalle's invariance principle. For simplicity, we define the auxiliary function $\mathscr{F}(\varsigma) = \varsigma - 1 - \ln \varsigma$ (defined for $\varsigma > 0$). By direct calculation, $\mathscr{F}(\varsigma)$ is strictly convex with a unique critical point at $\varsigma = 1$, thus implying $\mathscr{F}(\varsigma) \geq 0$ and $\mathscr{F}(\varsigma) = 0$ only if $\varsigma = 1$.

Theorem 3.1. *Under the condition $R_0 < 1$, the infection-free equilibrium E_0 of Model* (1.2) *is globally attractive.*

Proof. The Lyapunov functional $V_1(t)$ is defined by the following:

$$\begin{aligned} V_1(t) &= k_1 x_0 \mathscr{F}\left(\frac{x(t)}{x_0}\right) + y(t) + \frac{(\alpha+d)R_0'}{k_2\sigma R_0}c(t) + \frac{(\alpha+d)R_0''}{k_3 k R_0}v(t) + \frac{p}{\eta}z(t) \\ &\quad + \beta_1 \int_0^{T_1} f_1(\tau_1)e^{-m_1\tau_1}\int_{t-\tau_1}^{t}\frac{x(s)c(s)}{1+mc(s)}\mathrm{d}s\mathrm{d}\tau_1 + \beta_2\int_0^{T_1} f_1(\tau_1)e^{-m_1\tau_1}\int_{t-\tau_1}^{t}\frac{x(s)v(s)}{1+nv(s)}\mathrm{d}s\mathrm{d}\tau_1 \\ &\quad + \frac{(\alpha+d)R_0'}{k_2 R_0}\int_0^{T_2} f_2(\tau_2)e^{-m_2\tau_2}\int_{t-\tau_2}^{t} y(s)\mathrm{d}s\mathrm{d}\tau_2 + \frac{(\alpha+d)R_0''}{k_3 R_0}\int_0^{T_3} f_3(\tau_3)e^{-m_3\tau_3}\int_{t-\tau_3}^{t} y(s)\mathrm{d}s\mathrm{d}\tau_3. \end{aligned}$$

By differentiating $V_1(t)$ along the solutions of (1.2) that remain strictly positive, while implementing the parameter constraint $\lambda = \mu x_0$, we derive the following:

$$\begin{aligned} \dot{V}_1(t) &= k_1\left(1-\frac{x_0}{x(t)}\right)\left[\lambda - \frac{\beta_1 x(t)c(t)}{1+mc(t)} - \frac{\beta_2 x(t)v(t)}{1+nv(t)} - \mu x(t)\right] + \int_0^{T_1}\frac{f_1(\tau_1)e^{-m_1\tau_1}\beta_1 x(t-\tau_1)c(t-\tau_1)}{1+mc(t-\tau_1)}\mathrm{d}\tau_1 \\ &\quad + \int_0^{T_1}\frac{f_1(\tau_1)e^{-m_1\tau_1}\beta_2 x(t-\tau_1)v(t-\tau_1)}{1+nv(t-\tau_1)}\mathrm{d}\tau_1 - (\alpha+d)y(t) - py(t)z(t) \\ &\quad + \frac{(\alpha+d)R_0'}{k_2\sigma R_0}\left[\sigma\int_0^{T_2} f_2(\tau_2)e^{-m_2\tau_2}y(t-\tau_2)\mathrm{d}\tau_2 - qc(t)\right] \\ &\quad + \frac{(\alpha+d)R_0''}{k_3 k R_0}\left[k\int_0^{T_3} f_3(\tau_3)e^{-m_3\tau_3}y(t-\tau_3)\mathrm{d}\tau_3 - \gamma v(t)\right] + \frac{p}{\eta}\left[\frac{\eta y(t)z(t)}{1+\xi z(t)} - bz(t)\right] \\ &\quad + \frac{k_1\beta_1 x(t)c(t)}{1+mc(t)} - \int_0^{T_1}\frac{f_1(\tau)e^{-m_1\tau_1}\beta_1 x(t-\tau_1)c(t-\tau_1)}{1+mc(t-\tau_1)}\mathrm{d}\tau_1 \\ &\quad + \frac{k_1\beta_2 x(t)v(t)}{1+nv(t)} - \int_0^{T_1}\frac{f_1(\tau_1)e^{-m_1\tau_1}\beta_2 x(t-\tau_1)v(t-\tau_1)}{1+nv(t-\tau_1)}\mathrm{d}\tau_1 \\ &\quad + \frac{(\alpha+d)R_0'}{k_2 R_0}\left[k_2 y(t) - \int_0^{T_2} f_2(\tau_2)e^{-m_2\tau_2}y(t-\tau_2)\mathrm{d}\tau_2\right] \\ &\quad + \frac{(\alpha+d)R_0''}{k_3 R_0}\left[k_3 y(t) - k\int_0^{T_3} f_3(\tau_3)e^{-m_3\tau_3}y(t-\tau_3)\mathrm{d}\tau_3\right] \\ &= -\frac{k_1\mu(x(t)-x_0)^2}{x(t)} + \frac{\lambda k_1}{\mu R_0}\left[\frac{\beta_1 c(t)}{1+mc(t)} + \frac{\beta_2 v(t)}{1+nv(t)}\right](R_0-1) \\ &\quad - \frac{\lambda k_1\beta_1 m(c(t))^2}{\mu R_0(1+mc(t))} - \frac{\lambda k_1\beta_2 n(v(t))^2}{\mu R_0(1+nv(t))} - \frac{pbz(t)}{\eta} - \frac{\xi p y(t)(z(t))^2}{1+\xi z(t)}. \end{aligned}$$

Clearly, we have $\dot{V}_1(t) \leq 0$ if $R_0 < 1$. Moreover, $\dot{V}_1(t) = 0$ holds if and only if $x(t) = x_0$, and $y(t) = c(t) = v(t) = z(t) = 0$. Therefore, the maximal invariant set contained in $\{\dot{V}_1(t) = 0\}$ is precisely $\{E_0\}$. Therefore, the global attractivity of E_0 is concluded via LaSalle's invariance principle. □

Theorem 3.2. *Under the condition $R_0 > 1$ and $R_1 < 1$, the immunity-inactivated equilibrium E_1 of Model* (1.2) *is globally attractive.*

Proof. The Lyapunov functional is given by the following:

$$\begin{aligned}
V_2(t) &= x_1\mathscr{F}\left(\frac{x(t)}{x_1}\right) + \frac{y_1}{k_1}\mathscr{F}\left(\frac{y(t)}{y_1}\right) + \frac{\beta_1\widetilde{H}_1c_1}{\sigma k_2y_1}\mathscr{F}\left(\frac{c(t)}{c_1}\right) + \frac{\beta_2\widetilde{H}_2v_1}{kk_3y_1}\mathscr{F}\left(\frac{v(t)}{v_1}\right) + \frac{p}{\eta k_1}z(t)\\
&\quad + \frac{\beta_1\widetilde{H}_1}{k_1}\int_0^{T_1} f_1(\tau_1)e^{-m_1\tau_1}\int_{t-\tau_1}^{t}\mathscr{F}\left(\frac{H_1(s)}{\widetilde{H}_1}\right)\mathrm{d}s\mathrm{d}\tau_1\\
&\quad + \frac{\beta_2\widetilde{H}_2}{k_1}\int_0^{T_1} f_1(\tau_1)e^{-m_1\tau_1}\int_{t-\tau_1}^{t}\mathscr{F}\left(\frac{H_2(s)}{\widetilde{H}_2}\right)\mathrm{d}s\mathrm{d}\tau_1\\
&\quad + \frac{\beta_1\widetilde{H}_1}{k_2}\int_0^{T_2} f_2(\tau_2)e^{-m_2\tau_2}\int_{t-\tau_2}^{t}\mathscr{F}\left(\frac{y(s)}{y_1}\right)\mathrm{d}s\mathrm{d}\tau_2\\
&\quad + \frac{\beta_2\widetilde{H}_2}{k_3}\int_0^{T_3} f_3(\tau_3)e^{-m_3\tau_3}\int_{t-\tau_3}^{t}\mathscr{F}\left(\frac{y(s)}{y_1}\right)\mathrm{d}s\mathrm{d}\tau_3,
\end{aligned}$$

where $\widetilde{H}_1 = \frac{x_1c_1}{1+mc_1}, \widetilde{H}_2 = \frac{x_1v_1}{1+nv_1}, H_1(t) = \frac{x(t)c(t)}{1+mc(t)}$, and $H_2(t) = \frac{x(t)v(t)}{1+nv(t)}$. By determining the derivative of $V_2(t)$ for the positive solutions of Model (1.2) and applying

$$\lambda = \beta_1\widetilde{H}_1 + \beta_2\widetilde{H}_2 + \mu x_1, \quad k_1(\beta_1\widetilde{H}_1 + \beta_2\widetilde{H}_2) = (\alpha + d)y_1, \quad k_2\sigma y_1 = qc_1,\ k_3ky_1 = \gamma v_1,$$

we obtain the following:

$$\begin{aligned}
\dot{V}_2(t) &= \left(1 - \frac{x_1}{x(t)}\right)[\lambda - \beta_1H_1(t) - \beta_2H_2(t) - \mu x(t)] + \frac{1}{k_1}\left(1 - \frac{y_1}{y(t)}\right)\left[\int_0^{T_1} f_1(\tau_1)e^{-m_1\tau_1}\beta_1H_1(t-\tau_1)\mathrm{d}\tau_1\right.\\
&\quad \left. + \int_0^{T_1} f_1(\tau_1)e^{-m_1\tau_1}\beta_2H_2(t-\tau_1)\mathrm{d}\tau_1 - (\alpha + d)y(t) - py(t)z(t)\right]\\
&\quad + \frac{\beta_1\widetilde{H}_1}{k_2\sigma y_1}\left(1 - \frac{c_1}{c(t)}\right)\left[\sigma\int_0^{T_2} f_2(\tau_2)e^{-m_2\tau_2}y(t-\tau_2)\mathrm{d}\tau_2 - qc(t)\right]\\
&\quad + \frac{\beta_2\widetilde{H}_2}{k_3ky_1}\left(1 - \frac{v_1}{v(t)}\right)\left[k\int_0^{T_3} f_3(\tau_3)e^{-m_3\tau_3}y(t-\tau_3)\mathrm{d}\tau_3 - \gamma v(t)\right] + \frac{p}{\eta k_1}\left[\frac{\eta y(t)z(t)}{1+\xi z(t)} - bz(t)\right]\\
&\quad + \beta_1\widetilde{H}_1\left(\frac{H_1(t)}{\widetilde{H}_1} - \ln\frac{H_1(t)}{\widetilde{H}_1}\right) - \frac{\beta_1\widetilde{H}_1}{k_1}\int_0^{T_1} f_1(\tau_1)e^{-m_1\tau_1}\left(\frac{H_1(t-\tau_1)}{\widetilde{H}_1} - \ln\frac{H_1(t-\tau_1)}{\widetilde{H}_1}\right)\mathrm{d}\tau_1\\
&\quad + \beta_2\widetilde{H}_2\left(\frac{H_2(t)}{\widetilde{H}_2} - \ln\frac{H_2(t)}{\widetilde{H}_2}\right) - \frac{\beta_2\widetilde{H}_2}{k_1}\int_0^{T_1} f_1(\tau_1)e^{-m_1\tau_1}\left(\frac{H_2(t-\tau_1)}{\widetilde{H}_2} - \ln\frac{H_2(t-\tau_1)}{\widetilde{H}_2}\right)\mathrm{d}\tau_1\\
&\quad + \beta_1\widetilde{H}_1\left(\frac{y(t)}{y_1} - \ln\frac{y(t)}{y_1}\right) - \frac{\beta_1\widetilde{H}_1}{k_2}\int_0^{T_2} f_2(\tau_2)e^{-m_2\tau_2}\left(\frac{y(t-\tau_2)}{y_1} - \ln\frac{y(t-\tau_2)}{y_1}\right)\mathrm{d}\tau_2\\
&\quad + \beta_2\widetilde{H}_2\left(\frac{y(t)}{y_1} - \ln\frac{y(t)}{y_1}\right) - \frac{\beta_2\widetilde{H}_2}{k_3}\int_0^{T_3} f_3(\tau_3)e^{-m_3\tau_3}\left(\frac{y(t-\tau_3)}{y_1} - \ln\frac{y(t-\tau_3)}{y_1}\right)\mathrm{d}\tau_3
\end{aligned}$$

$$
\begin{aligned}
= & -\frac{\mu(x(t)-x_1)^2}{x(t)} - \beta_1\widetilde{H}_1\left[\mathscr{F}\left(\frac{x_1}{x(t)}\right)+\mathscr{F}\left(\frac{1+mc(t)}{1+mc_1}\right)\right] - \beta_2\widetilde{H}_2\left[\mathscr{F}\left(\frac{x_1}{x(t)}\right)+\mathscr{F}\left(\frac{1+nv(t)}{1+nv_1}\right)\right] \\
& -\frac{\beta_1\widetilde{H}_1}{k_1}\int_0^{T_1} f_1(\tau_1)e^{-m_1\tau_1}\mathscr{F}\left(\frac{y_1H_1(t-\tau_1)}{y(t)\widetilde{H}_1}\right)\mathrm{d}\tau_1 - \frac{\beta_2\widetilde{H}_2}{k_1}\int_0^{T_1} f_1(\tau_1)e^{-m_1\tau_1}\mathscr{F}\left(\frac{y_1H_2(t-\tau_1)}{y(t)\widetilde{H}_2}\right)\mathrm{d}\tau_1 \\
& -\frac{\beta_1\widetilde{H}_1}{k_2}\int_0^{T_2} f_2(\tau_2)e^{-m_2\tau_2}\mathscr{F}\left(\frac{c_1y(t-\tau_2)}{c(t)y_1}\right)\mathrm{d}\tau_2 - \frac{\beta_2\widetilde{H}_2}{k_3}\int_0^{T_3} f_3(\tau_3)e^{-m_3\tau_3}\mathscr{F}\left(\frac{v_1y(t-\tau_3)}{v(t)y_1}\right)\mathrm{d}\tau_3 \\
& -\frac{m\beta_1x_1(c(t)-c_1)^2}{(1+mc(t))(1+mc_1)^2} - \frac{n\beta_2x_1(v(t)-v_1)^2}{(1+nv(t))(1+nv_1)^2} - \frac{\xi py(t)(z(t))^2}{k_1(1+\xi z(t))} + \frac{pbz(t)}{k_1\eta}(R_1-1).
\end{aligned}
$$

Therefore, we have $\dot{V}_2(t) \leq 0$. Moreover, the equality condition is satisfied if and only if $\frac{x_1}{x(t)} = \frac{y_1H_1(t-\tau_1)}{y(t)\widetilde{H}_1} = \frac{y_1H_2(t-\tau_1)}{y(t)\widetilde{H}_2} = \frac{c_1y(t-\tau_2)}{c(t)y_1} = \frac{v_1y(t-\tau_3)}{v(t)y_1} = \frac{1+mc(t)}{1+mc_1} = \frac{1+nv(t)}{1+nv_1} = \frac{c(t)}{c_1} = \frac{v(t)}{v_1} = 1$ and $z(t) = 0$. By simple calculation, the maximum invariant set contained in $\{\dot{V}_2(t) = 0\}$ is verified to be $\{E_1\}$. Therefore, LaSalle's invariance principle is employed to demonstrate the global attractivity of E_1. □

Theorem 3.3. *Under the condition $R_0 > 1$ and $R_1 > 1$, the immunity-activated equilibrium E^* of Model* (1.2) *is globally attractive.*

Proof. The Lyapunov functional $V_3(t)$ is constructed using the following expression:

$$
\begin{aligned}
V_3(t) = & \; x^*\mathscr{F}\left(\frac{x(t)}{x^*}\right) + \frac{y^*}{k_1}\mathscr{F}\left(\frac{y(t)}{y^*}\right) + \frac{\beta_1H_1^*c^*}{\sigma k_2y^*}\mathscr{F}\left(\frac{c(t)}{c^*}\right) + \frac{\beta_2H_2^*v^*}{kk_3y^*}\mathscr{F}\left(\frac{v(t)}{v^*}\right) \\
& + \frac{p}{\eta k_1}\int_{z^*}^{z(t)}\frac{(1+\xi s)(s-z^*)}{z(t)}\mathrm{d}s + \frac{\beta_1H_1^*}{k_1}\int_0^{T_1} f_1(\tau_1)e^{-m_1\tau_1}\int_{t-\tau_1}^{t}\mathscr{F}\left(\frac{H_1(s)}{H_1^*}\right)\mathrm{d}s\mathrm{d}\tau_1 \\
& + \frac{\beta_2H_2^*}{k_1}\int_0^{T_1} f_1(\tau_1)e^{-m_1\tau_1}\int_{t-\tau_1}^{t}\mathscr{F}\left(\frac{H_2(s)}{H_2^*}\right)\mathrm{d}s\mathrm{d}\tau_1 \\
& + \frac{\beta_1H_1^*}{k_2}\int_0^{T_2} f_2(\tau_2)e^{-m_2\tau_2}\int_{t-\tau_2}^{t}\mathscr{F}\left(\frac{y(s)}{y^*}\right)\mathrm{d}s\mathrm{d}\tau_2 + \frac{\beta_2H_2^*}{k_3}\int_0^{T_3} f_3(\tau_3)e^{-m_3\tau_3}\int_{t-\tau_3}^{t}\mathscr{F}\left(\frac{y(s)}{y^*}\right)\mathrm{d}s\mathrm{d}\tau_3,
\end{aligned}
$$

where $H_1^* = \frac{x^*c^*}{1+mc^*}$, $H_2^* = \frac{x^*v^*}{1+nv^*}$, $H_1(t) = \frac{x(t)c(t)}{1+mc(t)}$, and $H_2(t) = \frac{x(t)v(t)}{1+nv(t)}$. By evaluating the derivative of $V_3(t)$ along solution trajectories of (1.2) and applying

$$
\lambda = \beta_1H_1^*+\beta_2H_2^*+\mu x^*,\;\; k_1(\beta_1H_1^*+\beta_2H_2^*) = (\alpha+d)y^*+py^*z^*,\;\; k_2\sigma y^* = qc^*,\;\; k_3ky^* = \gamma v^*,\;\; \eta y^* = b(1+\xi z^*),
$$

we derive the following:

$$
\begin{aligned}
\dot{V}_3(t) = & \left(1-\frac{x^*}{x(t)}\right)[\lambda-\beta_1H_1(t)-\beta_2H_2(t)-\mu x(t)] + \frac{1}{k_1}\left(1-\frac{y^*}{y(t)}\right)\left[\int_0^{T_1} f_1(\tau_1)e^{-m_1\tau_1}\beta_1H_1(t-\tau_1)\mathrm{d}\tau_1\right. \\
& \left. + \int_0^{T_1} f_1(\tau_1)e^{-m_1\tau_1}\beta_2H_2(t-\tau_1)\mathrm{d}\tau_1 - (\alpha+d)y(t) - py(t)z(t)\right] \\
& + \frac{\beta_1H_1^*}{k_2\sigma y^*}\left(1-\frac{c^*}{c(t)}\right)\left[\sigma\int_0^{T_2} f_2(\tau_2)e^{-m_2\tau_2}y(t-\tau_2)\mathrm{d}\tau_2 - qc(t)\right] \\
& + \frac{\beta_2H_2^*}{k_3ky^*}\left(1-\frac{v^*}{v(t)}\right)\left[k\int_0^{T_3} f_3(\tau_3)e^{-m_3\tau_3}y(t-\tau_3)\mathrm{d}\tau_3 - \gamma v(t)\right]
\end{aligned}
$$

$$
\begin{aligned}
&+\frac{p(1+\xi z(t))(z(t)-z^*)}{\eta k_1 z(t)}\left[\frac{\eta y(t)z(t)}{1+\xi z(t)}-bz(t)\right]\\
&+\beta_1 H_1^*\left(\frac{H_1(t)}{H_1^*}-\ln\frac{H_1(t)}{H_1^*}\right)-\frac{\beta_1 H_1^*}{k_1}\int_0^{T_1} f_1(\tau_1)e^{-m_1\tau_1}\left(\frac{H_1(t-\tau_1)}{H_1^*}-\ln\frac{H_1(t-\tau_1)}{H_1^*}\right)\mathrm{d}\tau\\
&+\beta_2 H_2^*\left(\frac{H_2(t)}{H_2^*}-\ln\frac{H_2(t)}{H_2^*}\right)-\frac{\beta_2 H_2^*}{k_1}\int_0^{T_1} f_1(\tau_1)e^{-m_1\tau_1}\left(\frac{H_2(t-\tau_1)}{H_2^*}-\ln\frac{H_2(t-\tau_1)}{H_2^*}\right)\mathrm{d}\tau\\
&+\beta_1 H_1^*\left(\frac{y(t)}{y^*}-\ln\frac{y(t)}{y^*}\right)-\frac{\beta_1 H_1^*}{k_2}\int_0^{T_2} f_2(\tau_2)e^{-m_2\tau_2}\left(\frac{y(t-\tau_2)}{y^*}-\ln\frac{y(t-\tau_2)}{y^*}\right)\mathrm{d}\tau_2\\
&+\beta_2 H_2^*\left(\frac{y(t)}{y^*}-\ln\frac{y(t)}{y^*}\right)-\frac{\beta_2 H_2^*}{k_3}\int_0^{T_3} f_3(\tau_3)e^{-m_3\tau_3}\left(\frac{y(t-\tau_3)}{y^*}-\ln\frac{y(t-\tau_3)}{y^*}\right)\mathrm{d}\tau_3\\
=\;&-\frac{\mu(x(t)-x^*)^2}{x(t)}-\beta_1 H_1^*\left[\mathscr{F}\left(\frac{x^*}{x(t)}\right)+\mathscr{F}\left(\frac{1+mc(t)}{1+mc^*}\right)\right]-\beta_2 H_2^*\left[\mathscr{F}\left(\frac{x^*}{x(t)}\right)+\mathscr{F}\left(\frac{1+nv(t)}{1+nv^*}\right)\right]\\
&-\frac{\beta_1 H_1^*}{k_1}\int_0^{T_1} f_1(\tau_1)e^{-m_1\tau_1}\mathscr{F}\left(\frac{y^*H_1(t-\tau_1)}{y(t)H_1^*}\right)\mathrm{d}\tau_1-\frac{\beta_2 H_2^*}{k_1}\int_0^{T_1} f_1(\tau_1)e^{-m_1\tau_1}\mathscr{F}\left(\frac{y^*H_2(t-\tau_1)}{y(t)H_2^*}\right)\mathrm{d}\tau_1\\
&-\frac{\beta_1 H_1^*}{k_2}\int_0^{T_2} f_2(\tau_2)e^{-m_2\tau_2}\mathscr{F}\left(\frac{c^*y(t-\tau_2)}{c(t)y^*}\right)\mathrm{d}\tau_2-\frac{\beta_2 H_2^*}{k_3}\int_0^{T_3} f_3(\tau_3)e^{-m_3\tau_3}\mathscr{F}\left(\frac{v^*y(t-\tau_3)}{v(t)y^*}\right)\mathrm{d}\tau_3\\
&-\frac{m\beta_1 x^*(c(t)-c^*)^2}{(1+mc(t))(1+mc^*)^2}-\frac{n\beta_2 x^*(v(t)-v^*)^2}{(1+nv(t))(1+nv^*)^2}-\frac{\xi p y^*(z(t)-z^*)^2}{k_1}.
\end{aligned}
$$

Therefore, $\dot{V}_3(t) \le 0$. Furthermore, $\dot{V}_3(t) = 0$ if and only if $\frac{x^*}{x(t)} = \frac{y^*H_1(t-\tau_1)}{y(t)H_1^*} = \frac{y^*H_2(t-\tau_1)}{y(t)H_2^*} = \frac{c^*y(t-\tau_2)}{c(t)y^*} = \frac{v^*y(t-\tau_3)}{v(t)y^*} = \frac{1+mc(t)}{1+mc^*} = \frac{1+nv(t)}{1+nv^*} = \frac{c(t)}{c^*} = \frac{v(t)}{v^*} = \frac{z(t)}{z^*} = 1$. A direct calculation establishes $\{E^*\}$ as the maximal invariant set for $\{\dot{V}_3(t) = 0\}$. Through LaSalle's invariance principle, the global attractivity of E^* is established. □

4. Numerical simulations

This section presents numerical simulations of the dynamical behavior of Model (1.2) through MATLAB implementations. The model parameters, adopted from [12], are set as $\lambda = 10, \beta_1 = 0.0012, \beta_2 = 0.001, \mu = 0.1, \alpha = 0.1, d = 0.75, p = 0.001, \sigma = 0.25, q = 0.1, k = 13, \gamma = 0.3, \eta = 0.33$, and $m_1 = m_2 = m_3 = 0.1$, with initial conditions $(50, 3, 60, 2, 450)$. The remaining parameters are specified in the corresponding numerical simulations. For simplicity in numerical implementation while preserving generality, we take $T_1 = T_2 = T_3 = T^*$ as identical delay parameters.

We begin our stability analysis by numerically confirming the global attractivity of the model's equilibrium points when the parameters are set as $T^* = 2$ and $m = n = \xi = 0.005$.

- The infection-free equilibrium E_0: When $\beta_1 = 0.00012, \beta_2 = 0.0001$, and $b = 0.32$ (low-transmission regime), the basic reproduction number is $R_0 = 0.4523 < 1$. As shown in Figure 1, the solution trajectories converge to $E_0(100, 0, 0, 0, 0)$, which is consistent with the global attractivity result established in Theorem 3.
- The immune-inactivated equilibrium E_1: When $\beta_1 = 0.0012, \beta_2 = 0.001$ (heightened transmission), and $b = 3$ (increased viral infectivity), we obtain $R_0 = 4.5228 > 1$ and

$R_1 = 0.5975 < 1$. Figure 2 numerically illustrates the convergence of solutions to the equilibrium $E_1(45.9851, 5.4317, 12.3743, 214.3993, 0)$, thus validating the theoretical results in Theorem 4.

- The immune-activated equilibrium E^*: Maintaining the elevated transmission rates ($\beta_1 = 0.0012, \beta_2 = 0.001$) while reducing infectivity to $b = 0.32$ produces $R_0 = 4.5228 > 1$ and $R_1 = 70.7128 > 1$. Figure 3 verifies the global attractivity of E^* as concluded in Theorem 5, with the corresponding steady-state values $(54.283, 3.1067, 7.075, 122.633, 440.785)$.

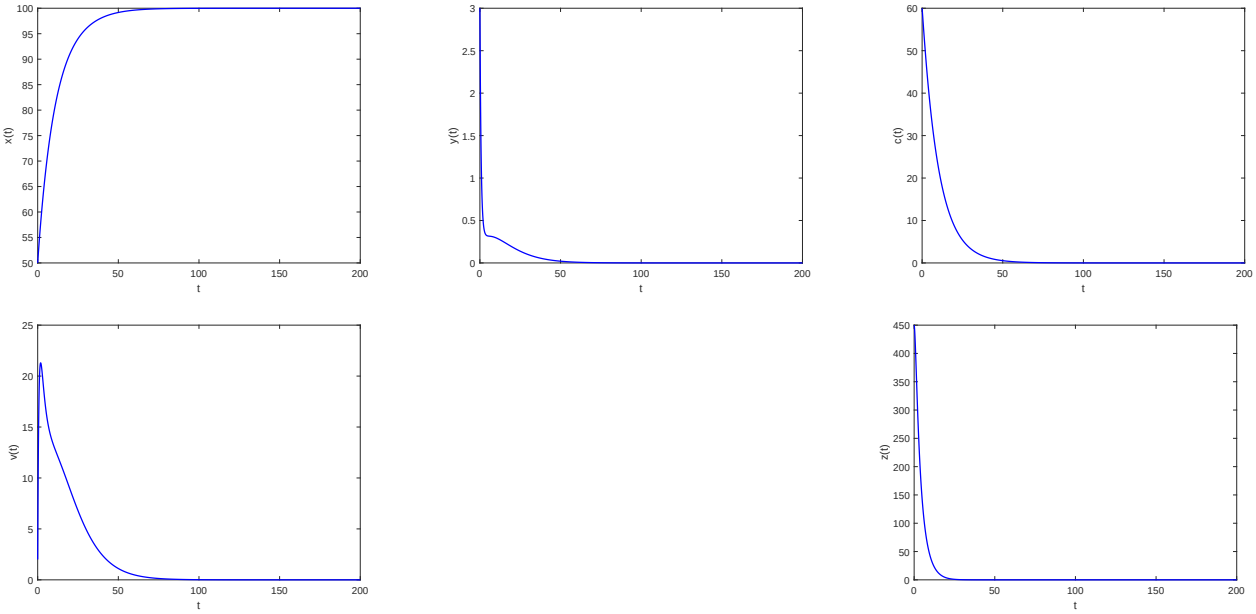

Figure 1. Phase portrait of Model (1.2) at infection-free equilibrium E_0 ($R_0 < 1$).

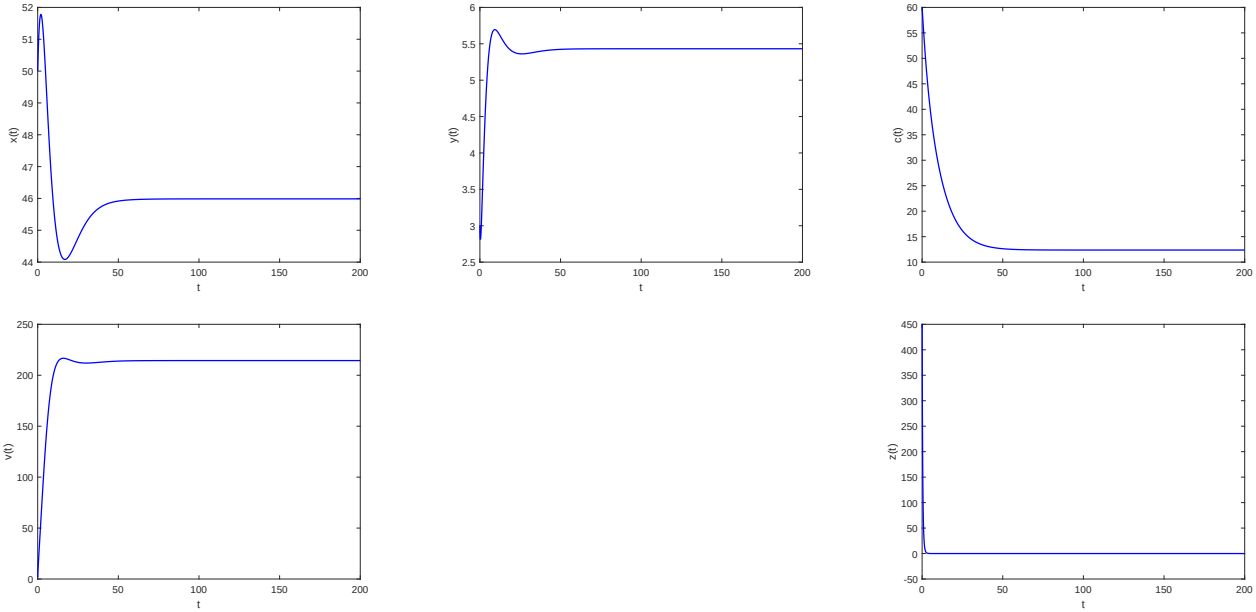

Figure 2. Phase portrait of Model (1.2) at immune-inactivated equilibrium E_1 ($R_0 > 1$ and $R_1 < 1$).

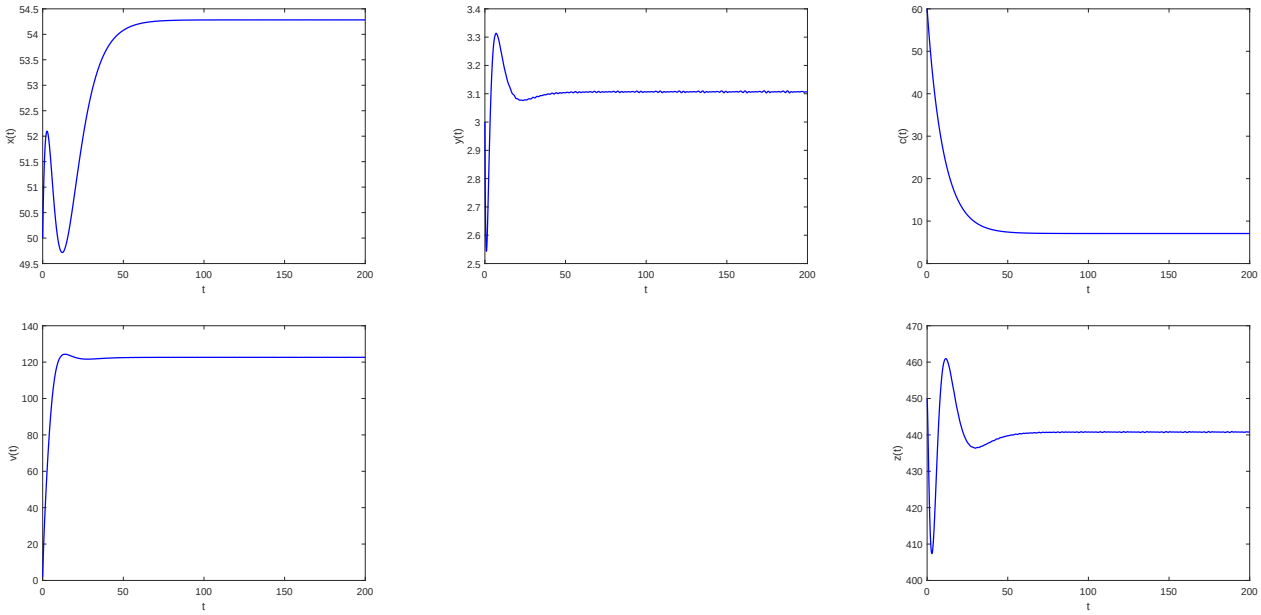

Figure 3. Phase portrait of Model (1.2) at immune-activated equilibrium E_1 ($R_0 > 1$ and $R_1 > 1$).

With the parameter b fixed at 0.32, we subsequently systematically investigate how variations in saturation constants (m, n) and a time delay (T^*) dynamically affect all system variables in Model (1.2). Under the conditions of $\xi = 0.005$ and $T^* = 2$, we perform numerical simulations to analyze how the system stability varies with the saturation constants m and n (Figure 4). The simulations demonstrate that as the saturation constants (m or n) increase, the population of uninfected CD4$^+$ T cells ($x(t)$) exhibits differential growth patterns, whereas the strength of infected cells ($y(t)$), inflammatory cytokines ($c(t)$), viral particles ($v(t)$), and CTLs ($z(t)$) all show consistent monotonic declines.

- With n fixed at 0.005, m increases from 0.005 to 0.5: $x(t)$ only marginally increases by 3.91% (from 54.2831 to 56.4052), whereas $y(t), c(t)$, and $v(t)$ exhibit synchronous decreases of 1.26%, and $z(t)$ demonstrates a slightly larger reduction of 1.83%.
- With m fixed at 0.005, n increases from 0.005 to 0.5: $x(t)$ exhibits a dramatic increase of 80.57% (from 54.2831 to 98.017). Meanwhile, $z(t)$ is completely depleted (decreasing to zero), thus indicating a more drastic elimination than the observed 94.4% reduction in $y(t), c(t)$, and $v(t)$.

Figure 4 shows that the saturation effect of inflammatory cytokine has minimal impact, whereas virus-cell saturation is pivotal for HIV treatment and requires precise modulation.

With parameters fixed at $T^* = 2$ and $m = n = 0.005$ (Figure 5), numerical simulations demonstrate that increasing the immune saturation parameter ξ (initially at $\xi = 0.005$) leads to a monotonic decline in uninfected CD4$^+$ T cell ($x(t)$) and CTLs ($z(t)$), whereas infected cells ($y(t)$), inflammatory cytokines ($c(t)$), and the viral load ($v(t)$)exhibit sustained growths. Remarkably, when ξ surpasses 0.5, all system variables approach steady-state concentrations, becoming largely insensitive to further increases in ξ. This behavior reflects an established equilibrium between viral replication and host immune suppression, thus illustrating the underlying mechanism of persistent viral propagation alongside compromised immune function during chronic infection.

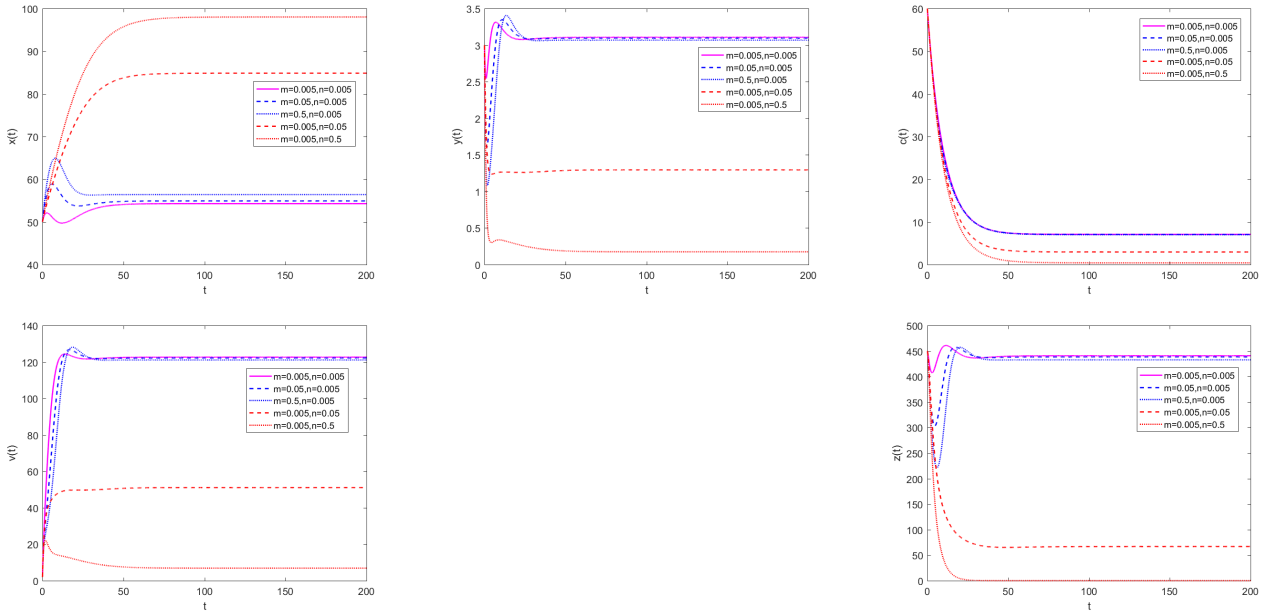

Figure 4. Phase portrait of Model (1.2) under different m and n.

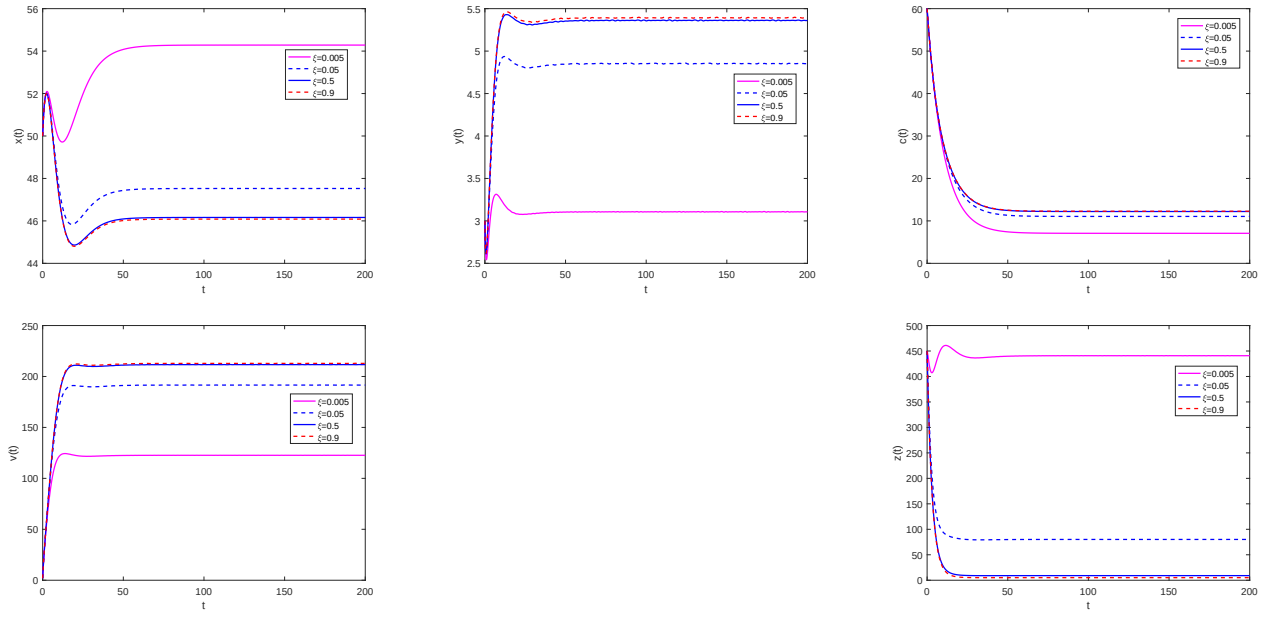

Figure 5. Phase portrait of Model (1.2) under different ξ.

When T^* varies from 2 to 100 under the fixed parameters $m = n = \xi = 0.005$, the simulations in Figure 6 demonstrate that increasing time delays results in the following: (i) substantial growth in uninfected CD4$^+$ T cells ($x(t)$); and (ii) marked reductions in infected cells ($y(t)$), inflammatory cytokines ($c(t)$), viral load ($v(t)$), and CTLs ($z(t)$). Notably, when the time delay exceeds 30 days ($T^* > 30$), all system variables reach a stable equilibrium with time-invariant concentrations. Numerical

simulations suggest that such time delays could be leveraged as potential intervention targets for HIV treatment. Furthermore, pharmacological modulation of these temporal dynamics may serve as an adjunct to current antiretroviral therapies when the system achieves a stable equilibrium at $T^* > 30$ days.

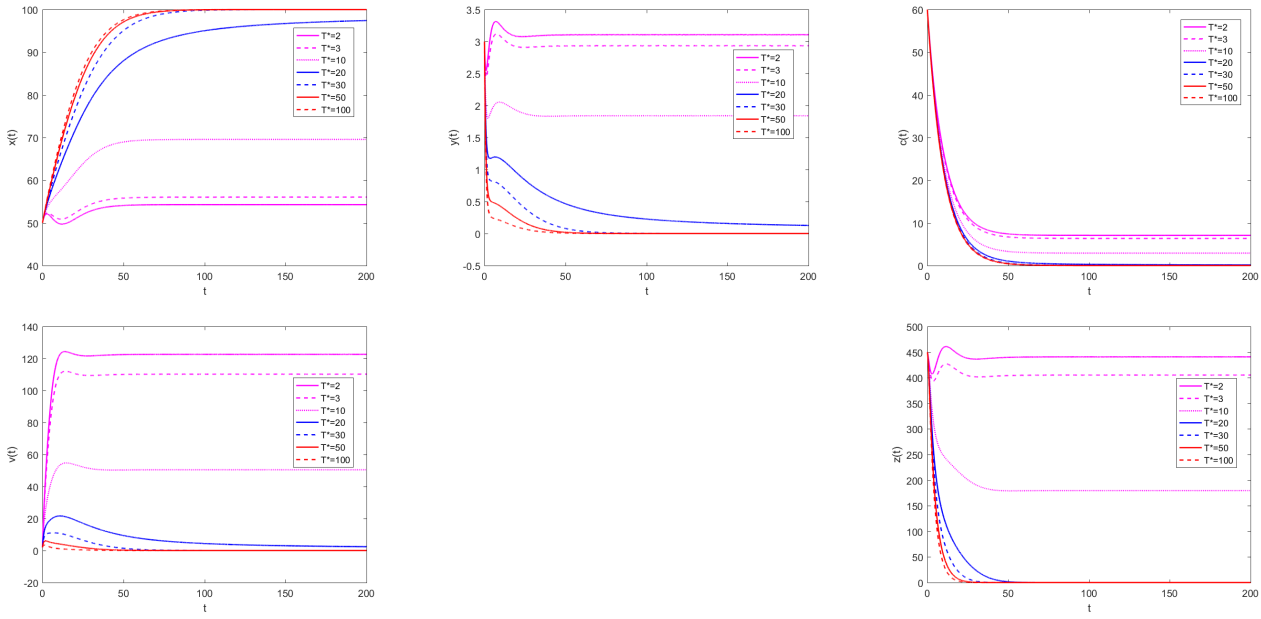

Figure 6. Phase portrait of Model (1.2) under different T^*.

Numerical simulations confirm that upregulating the immune saturation parameter ξ significantly drives the system variables toward AIDS progression. In Figure 7, we further examine how increasing either the saturation effect of the inflammatory cytokine parameter m or the virus-cell saturation n under ξ upregulation affects the system dynamics at distinct time delays ($T = 2$ vs $T = 20$).

- $T^* = 2$: Increasing the parameter n while simultaneously raising ξ induces a reversal in the system variable concentrations, thereby shifting the trend toward disease improvement.
- $T^* = 2$: Simultaneously increasing the parameter m with ξ produces a distinct system response: only uninfected target cell concentrations exhibit minor variations, while other variables remain essentially unchanged.
- $T^* = 20$: Increasing time delay induces rapid shifts in the system variables toward AIDS improvement. While raising the parameter ξ leaves these concentrations virtually unchanged, a simultaneous increase in n further enhances this therapeutic trend across all variables.

The numerical simulations of Figure 7 demonstrate that the saturation effect and time-delay characteristics in viral dynamics significantly influence HIV disease progression. Clinical outcomes may be significantly improved by combining viral saturation-targeting drugs with highly active antiretroviral therapy (HAART) and immunomodulation, while dynamically optimizing treatments based on time-delay characteristics.

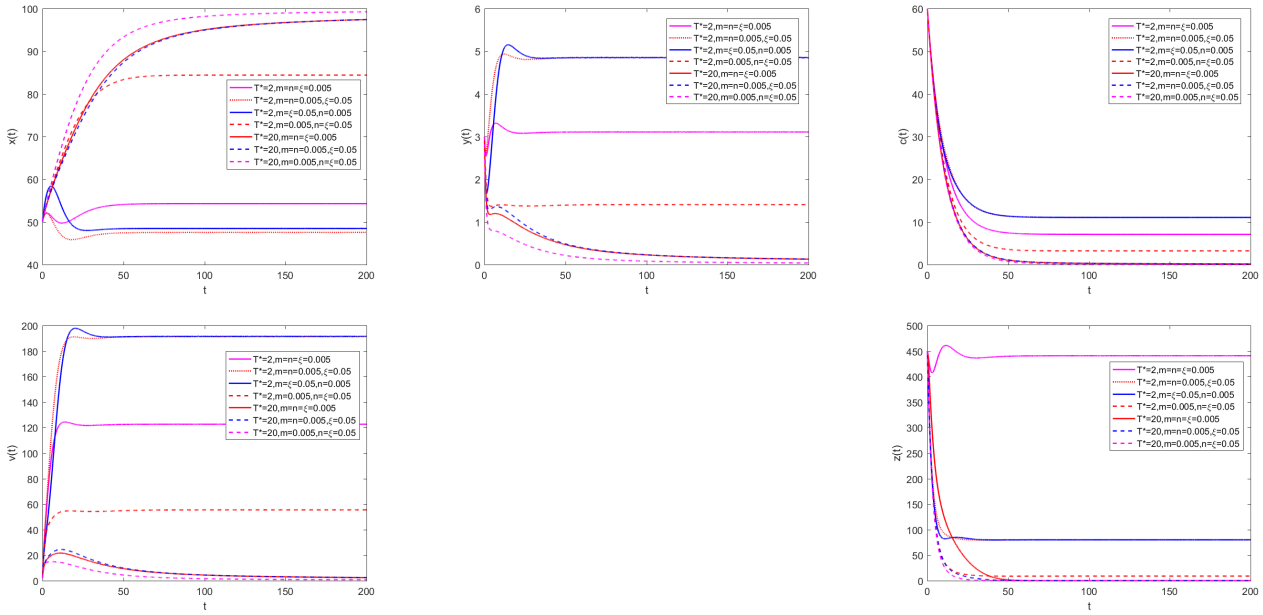

Figure 7. Parameter-dependent dynamics in Model (1.2): Effects of varying saturation parameters and time delays on system variables.

5. Conclusions and discussion

In this study, we formulated a cytokine-enhanced HIV model which accounts for saturated incidence rates and distributed delays. Through an analysis of distinct parameter regimes for the basic reproduction number (R_0) and immune reproduction number (R_1), we established the respective existence conditions for both the immune-inactivated and immune-activated equilibrium points. By systematically constructing Lyapunov functionals, we successfully demonstrated the global attractivity of all three equilibria.

Our numerical simulations confirm the global attractivity of all three equilibrium points under different parameter regimes. Subsequently, we conducted a comprehensive analysis of how variations in the saturation constants and time-delay parameters influence the dynamical behavior of the system variables. Our simulations revealed that while the virus-cell interaction saturation predominantly governs the system dynamics compared to the saturation effect of inflammatory cytokines in uninfected $CD4^+$ T cells, immune saturation simultaneously exerts a critical impairment on anti-HIV defense mechanisms. Notably, infection delays demonstrate biphasic therapeutic effects, thereby maintaining cellular homeostasis below a specific threshold but inducing pathological stabilization when exceeded. Most significantly, we found that the targeted enhancement of virus-cell saturation can effectively counteract these detrimental immune saturation effects.

The numerical simulations demonstrate that while an elevated saturation effect of inflammatory cytokines moderately influence the concentration dynamics of system variables, these effects become negligible when compared to the pronounced regulatory impact of the virus-cell saturation. This computational evidence strongly supports the clinical observation that pyroptosis remains particularly challenging to modulate in HIV treatment. These findings are consistent with [20], which indicates

that pyroptosis may still be triggered in virally suppressed patients by persistent inflammation or T cell receptor (TCR)-dependent antigen stimulation.

Our study demonstrates that the nonlinear saturation effects and time-delay characteristics in HIV infection not only significantly impact the disease pathogenesis but also represent highly potential targets for clinical intervention. These findings provide a theoretical foundation to optimize the treatment strategies, thus highlighting the necessity of incorporating these dynamic features into therapeutic design.

Author contributions

Cuifang Lv: Formal analysis, funding acquisition, methodology, software, validation, writing-original draft, writing-review, and editing; Xiaoyan Chen: Formal analysis, funding acquisition, methodology, writing-original draft, writing-review, and editing; Chaoxiong Du: Formal analysis, conceptualization, resources, writing-review and editing. All authors have read and approved the final version of the manuscript for publication.

Use of Generative-AI tools declaration

The authors declare that no Artificial Intelligence (AI) tools were used in the composition of this article.

Acknowledgments

This work was supported by the National Natural Science Foundation of China (12301186), the Changsha Normal University-Level Cultivation Program (Grant No. K84024031).

Conflict of interest

The authors declare that they have no known competing financial interests or personal relationships that could have appeared to influence the work reported in this paper.

References

1. L. G. Bekker, C. Beyrer, N. Mgodi, S. R. Lewin, S. Delany-Moretlwe, B. Taiwo, et al., HIV infection, *Nat. Rev. Dis. Primers*, **9** (2023), 42. https://doi.org/10.1038/s41572-023-00452-3
2. A. Mody, A. Sohn, C. Iwuji, R. K. J. Tan, F. Venter, E. H. Geng, HIV epidemiology, prevention, treatment, and implementation strategies for public health, *Lancet*, **403** (2023), 471–492. https://doi.org/10.1016/S0140-6736(23)01381-8
3. G. Doitsh, N. L. Galloway, X. Geng, Z. Y. Yang, K. M. Monroe, O. Zepeda, et al., Cell death by pyroptosis drives CD4 T-cell depletion in HIV-1 infection, *Nature*, **505** (2014), 509–514. https://doi.org/10.1038/nature12940
4. J. H. Xu, Dynamic analysis of a cytokine-enhanced viral infection model with infection age, *Math. Biosci. Eng.*, **20** (2023), 8666–8684. https://doi.org/10.3934/mbe.2023380

5. S. P. Wang, P. Hottz, M. Schechter, L. B. Rong, Modeling the slow $CD4^+$ T cell decline in HIV-infected individuals, *PLoS. Comput. Biol.*, **11** (2015), 1004665. https://doi.org/10.1371/journal.pcbi.1004665

6. Y. Jiang, T. Q. Zhang, Global stability of a cytokine-enhanced viral infection model with nonlinear incidence rate and time delays, *Appl. Math. Lett.*, **132** (2022), 108110. https://doi.org/10.1016/j.aml.2022.108110

7. J. E. Schmitz, M. J. Kuroda, S. Santra, V. G. Sasseville, M. A. Simon, M. A. Lifton, et al., Control of viremia in simian immunodeficiency virus infection by $CD8^+$ lymphocytes, *Science*, **283** (1999), 857–860. https://doi.org/10.1126/science.283.5403.857

8. J. M. Conway, R. M. Ribeiro, Modeling the immune response to HIV infection, *Curr. Opin. Syst. Biol.*, **12** (2018), 61–69. https://doi.org/10.1016/j.coisb.2018.10.006

9. Q. R. Song, S. L. Wang, F. Xu, Robustness and bistability in a cytokine-enhanced viral infection model, *Appl. Math. Lett.*, **158** (2024), 109215. https://doi.org/10.1016/j.aml.2024.109215

10. T. Q. Zhang, X. N. Xu, X. Z. Wang, Dynamic analysis of a cytokine-enhanced viral infection model with time delays and CTL immune response, *Chaos Solitons Fract.*, **170** (2023), 113357. https://doi.org/10.1016/j.chaos.2023.113357

11. C. Chen, Y. G. Zhou, Z. J. Ye, Stability and optimal control of a cytokine-enhanced general HIV infection model with antibody immune response and CTLs immune response, *CMBBE*, **27** (2024), 2199–2230. https://doi.org/10.1080/10255842.2023.2275248

12. C. F. Lv, X. Y. Chen, C. X. Du, Global dynamics of a cytokine-enhanced viral infection model with distributed delays and optimal control analysis, *AIMS Math.*, **10** (2025), 9493–9515. https://doi.org/10.3934/math.2025438

13. G. Huang, Y. Takeuchi, W. B. Ma, Lyapunov functionals for delay differential equations of viral infections, *SIAM J. Appl. Math.*, **70** (2010), 2693–2708. https://doi.org/10.1137/090780821

14. W. Chen, Z. D. Teng, L. Zhang, Global dynamics for a drug-sensitive and drug-resistant mixed strains of HIV infection model with saturated incidence and distributed delays, *Appl. Math. Comput.*, **406** (2021), 126284. https://doi.org/10.1016/j.amc.2021.126284

15. S. Chowdhury, J. K. Ghosh, U. Ghosh, Co-infection dynamics between HIV-HTLV-I disease with the effects of Cytotoxic T-lymphocytes, saturated incidence rate and study of optimal control, *Math. Comput. Simul.*, **223** (2024), 195–218. https://doi.org/10.1016/j.matcom.2024.04.015

16. W. Chen, L. Zhang, N. Wang, Z. D. Teng, Bifurcation analysis and chaos for a double-strains HIV coinfection model with intracellular delays, saturated incidence and Logistic growth, *Math. Comput. Simul.*, **223** (2024), 617–641. https://doi.org/10.1016/j.matcom.2024.04.025

17. W. J. Li, L. A. Yang, J. D. Cao, Threshold dynamics of a degenerated diffusive incubation period host-pathogen model with saturation incidence rate, *Appl. Math. Lett.*, **160** (2025), 109312. https://doi.org/10.1016/j.aml.2024.109312

18. J. K. Hale, S. M. V. Lunel, *Introduction to functional differential equations*, New York: Springer Science & Business Media, 1993. https://doi.org/10.1007/978-1-4612-4342-7

19. H. L. Smith, *Monotone dynamical systems: An introduction to the theory of competitive and cooperative systems*, Providence, Rhode Island: American Mathematical Society, 1995. https://doi.org/10.1090/surv/041

20. C. Zhang, J. W. Song, H. H. Huang, X. Fan, L. Huang, J. N. Deng, et al., NLRP3 inflammasome induces CD4$^+$ T cell loss in chronically HIV-1 Cinfected patients, *J. Clin. Invest.*, **131** (2021), e138861. https://doi.org/10.1172/JCI138861